MATERIALS CHEMISTRY FRONTIERS

CCS 中国化学会 CHINESE CHEMICAL SOCIETY

ICCAS

ROYAL SOCIETY OF CHEMISTRY

Liquid-phase bottom-up synthesis of graphene nanoribbons

Journal:	*Materials Chemistry Frontiers*
Manuscript ID	QM-REV-08-2019-000519.R1
Article Type:	Review Article
Date Submitted by the Author:	28-Sep-2019
Complete List of Authors:	Yoon, Ki-Young; The University of Chicago Dong, Guangbin; The University of Chicago,

REVIEW

Liquid-phase bottom-up synthesis of graphene nanoribbons

Ki-Young Yoon, Guangbin Dong *

Received 00th January 20xx,
Accepted 00th January 20xx

DOI: 10.1039/x0xx00000x

Graphene nanoribbons (GNRs) — an emerging family of carbon-based semiconductors — can be precisely synthesised from small molecules such as benzene derivatives through bottom-up approaches. This review outlines a summary of the development of bottom-up synthesis of GNRs in liquid phase. The strategies are classified based on edge structures and widths of the materials, which are the crucial factors for properties of GNRs. In addition, views on challenges in the field and the future outlook are also provided.

1. Introduction

Organic semiconductors hold great promise for enabling inexpensive productions of printed electronics and flexible displays.[1-3] However, to realise more practical and efficient devices from organic semiconductors, it is important to achieve precise bandgap engineering, as well as better charge carrier mobility, solution processability, and synthetic scalability of these materials.[2, 4] In this context, graphene nanoribbons (GNRs), regarded as quasi-one-dimensional subunits of graphene, are considered to be a highly promising class of organic semiconductors. As a special type of conjugated polymers, GNRs possess non-zero band gap because of the lateral quantum confinement; yet, they could maintain sufficiently high charge-carrier mobility (>200 $cm^2V^{-1}s^{-1}$) stemming from their mother material, graphene.[5-7]

The electronic properties of GNRs including bandgap and charge-carrier mobility critically depend on their chemical structures, such as edge types (armchair, zigzag, cove, fjord, etc.), width and length of the materials.[8-10] To date, "top-down" approaches, such as lithographic cutting of graphene sheets, unzipping of carbon nanotubes, or sonochemical extraction, have been used to provide GNRs from higher dimensional carbon materials.[11] However, these methods produce a mixture of GNRs with different lengths, widths, and edge structures. In addition, it is extremely challenging to obtain narrow GNRs (<2 nm) via a top-down approach, whose bandgaps are expected to be similar with those of conventional silicon semiconductors (~1.1 eV).[10]

In contrast, the "bottom-up" approaches allow for control of the structures of GNRs, because the judicious design of monomer structures, after a polymerisation and/or a graphenisation, not only dictates widths and edge structures of GNRs but also permits precise doping at specific positions.[12-15] Currently, liquid-phase and surface-assisted syntheses constitute two different approaches for the "bottom-up" preparation of GNRs. The surfaced-assisted protocol prepares GNRs from organic monomers on conductive metal surfaces after annealing, which generally give materials of high quality that can be directly monitored by scanning tunneling microscopy (STM) or atomic force microscopy (AFM) without any casting process. It avoids dealing with the solubility issues of the GNRs formed. In addition, these efforts have led to better characterisation and understanding of the properties of GNRs.[12, 15] On the other hand, as a complementary technique, the liquid-phase bottom-up synthesis is beneficial for (potential large-area) device fabrication in terms of scalability and processability of GNRs. The liquid-phase synthesis is generally operated under milder conditions (e.g. much lower reaction temperature); as a consequence, various functional groups or side chains could be introduced by this approach.[12, 14]

Inspired by a number of excellent reviews/accounts on GNR synthesis,[7, 9-11, 14-23] this review is focused on liquid-phase bottom-up synthetic strategies and is categorised based on edge structures and widths, the crucial factors for properties of GNRs (Fig. 1). On-surface GNR syntheses and syntheses of polyaromatic hydrocarbons/nanoribbons have been reviewed previously,[15, 18, 22-28] and are beyond the scope of this article. As a general note, when relative molecular weights of polymers are mentioned, the number-average molecular weights (M_ns) based on polystyrene standards from size exclusion chromatography (SEC) are used in order to compare with one another in a fair manner.

2. Graphene nanoribbons with armchair edges

The properties of GNRs with armchair-shaped edges, namely armchair GNRs, have been most studied from theory.[8, 29-32] Since armchair GNRs with N=3k (semiconducting), 3k+1

Department of Chemistry, The University of Chemistry, Chicago, IL60637, USA
E-mail: gbdong@uchicago.edu
Footnotes relating to the title and/or authors should appear here.
Electronic Supplementary Information (ESI) available: [details of any supplementary information available should be included here]. See DOI: 10.1039/x0xx00000x

(semiconducting), and 3k+2 (semimetallic) — *N* is defined as the number of rows of atoms forming the ribbon width and k is an integer — are predicted to display different characteristics,[8, 32] syntheses of armchair GNRs in each family are summarised here. In addition to conventional *N*-armchair GNRs, other armchair-like GNRs are also covered in this section.

2.1 *N*=3k Armchair graphene nanoribbons

***N*=9 armchair GNRs.** In 2000, Müllen reported an A_2B_2-type Diels–Alder polymerisation of dicyclopentadienone **M1c** with 1,4-diethynylbenzene (**M1a**) (Fig. 2). Subsequent cyclodehydrogenation of the resulting polymer (**P1a**) ($AlCl_3$, $Cu(OTf)_2$) resulted in an array of nanographenes (**G1a**) rather than a (continuous) GNR structure.[33] To prepare a continuous GNR structure, the same group later replaced the monomer from **M1a** to 1,4-diethynyl-2,5-di(4'-tert-butylphenyl)benzene (**M1b**), and the same polymerisation reaction afforded branched polyphenylenes (**P1b**) that contain three isomeric polymeric units (*trans*, linear, *cis*). The following cyclodehydrogenation of **P1b** with $FeCl_3$ yielded a kinked GNR (**G1b**) with an unclear absorption onset point corresponding to the optical bandgap of ~1.1 eV.[34]

In 2008, Müllen developed a seminal synthetic route to offer a linear armchair GNR via an A_2B_2-type Suzuki–Miyaura polymerisation of diiodobenzene **M2a** with bis(boronic ester) compound **M2b** (Fig. 3a).[35] Each monomer contained bulky 3,7-dimethyloctyl groups as side-chains to increase the processability of armchair GNRs. The resulting poly(*p*-phenylene)(PPP, **P2**) (M_n=13.9 kDa and $Đ$=1.2 after Soxhlet extraction, where $Đ$ is a molar mass dispersity (M_w/M_n)) was graphenised (94% efficiency) in the presence of $FeCl_3$ to generate the first well-defined *N*=9 armchair GNR (**G2**) with a length up to 12 nm. The relatively short **G2** presented excellent dispersity in common organic solvents; it possessed a relatively large optical bandgap of ~2.2 eV.

In 2016, our group developed a new synthetic route to *N*=9 armchair GNR via an *AB*-type Suzuki–Miyaura polymerisation based on a simple triaryl monomer (**M3**) (Fig. 3b).[36] The monomer can be easily prepared in 4 steps from 1,2-dibromobenzene. The polymerisation afforded a higher-molecular-weight PPP (**P3**) of M_n=30.6 kDa $Đ$=1.4 (after Soxhlet extraction) with excellent solubility. The oxidative cyclodehydrogenation with 2,3-dichloro-5,6-dicyanobenzoquinone (DDQ) and triflic acid (TfOH) transformed **P3** to a longer armchair GNR (**G3,** 99% graphenisation efficiency) with an optical bandgap of ~1.1 eV. The DDQ/TfOH condition was found to be more efficient and selective for cyclodehydrogenation than $FeCl_3$ in this case. The bandgap discrepancy between similar GNRs (**G2** and **G3**) infers that, besides width and edge structures, length (due to the finite-length effect)[37] and/or structural integrity of GNRs could also affect bandgaps.

***N*=18 armchair GNRs.** Feng, Müllen, and Samori in 2014 prepared *N*=18 armchair GNRs (**G4**) and then blended it with P3HT for OFET application because *N*=18 armchair GNR was expected to have an ionisation energy close to that of P3HT.[38] **G4** was produced by an *AA*-type Yamamoto polymerisation of dichloride **M4**, followed by the oxidative cyclodehydrogenation with $FeCl_3$ (Fig. 4). **G4** with a length up to 10 nm, made from **P4** (M_n=7.4 kDa, $Đ$=1.4), was detected by MALDI-TOF MS. The optical bandgap, which is theoretically predicted to be smaller than that of the narrower *N*=9 armchair GNR (*vide supra*, 1.1 eV for **G3**),[8] was measured to be 1.6 eV, and this could be possibly due to the short length of **G4**.[37] The fabricated device of P3HT with 24wt% **G4** displayed increased field-effect mobility (3.3×10^{-2} $cm^2V^{-1}s^{-1}$), compared to that of pristine P3HT (7.3×10^{-3} $cm^2V^{-1}s^{-1}$).

***N*=12 armchair GNR.** In 2016, Rubin reported a unique method to prepare an *N*=12 armchair GNR through crystal topochemical polymerisation (Fig. 5).[39] The crystal topochemical polymerisation is not a typical wet chemistry process but can be still regarded as liquid-phase bottom-up synthesis of GNRs rather than on-surface synthesis, given that crystals are grown in solution and polymerisation occurs without metal surfaces. Crystals of diacetylene monomers (**M5**) were polymerised under heat or light to give poly(diacetylene)s **P5**. The consecutive benzannulation and cyclodehydrogenation under an inert heating atmosphere (300 °C) yielded **G5**. While fused/cross-linked GNRs were observed, **G5** with an optical bandgap of 1.4 eV offered excellent properties for FET applications, including an average mobility of 0.15 $cm^2V^{-1}s^{-1}$ and an on–off current ratio of 5.

***N*=6 armchair GNRs.** *N*=6 armchair GNR, the narrowest member in the *N*=3k armchair GNR family, was prepared by our group in 2018 (Fig. 6).[40] Utilising simple monomers **M6a** and **M6d**, an A_2B_2-type Suzuki–Miyaura polymerisation yielded a PPP **P6a** (M_n=28.9 kDa $Đ$=1.71 after Soxhlet extraction). **P6a** was treated with DDQ and TfOH to afford **G6a** with the bandgap of 1.21 eV. Due to the modular synthetic approach, bandgap engineering of GNRs was achieved simply by using different monomers (e.g. **M6b** or **M6c**) instead of **M6a**. Just as donor-acceptor-type alternating conjugated copolymers, GNRs bearing electron-deficient heteroaryl units (**G6b** and **G6c**) possessed lower bandgaps than the pristine GNR (**G6a**) because of the intramolecular charge transfer. **G6b** and **G6c** also featured rare unsymmetrical edges. Capitalising on the heterocyclic moiety, post-functionalisation of **G6b** was realised via an N-directed C–H borylation (Fig. 7) toward **G6b-B**, which provided a further decreased optical bandgap (0.95 eV).

2.2 *N*=3k+1 Armchair graphene nanoribbons

***N*=13 armchair GNR.** In 2016, Loo fabricated a field-effect device exhibiting ambipolarity (hole: 1.3×10^{-7} $cm^2V^{-1}s^{-1}$, electron: 1.0×10^{-7} $cm^2V^{-1}s^{-1}$ at 78 K) in an accumulation mode, which was made of a novel *N*=13 armchair GNR.[41] This observation was similar to Jo's previous report with kinked GNRs (**G24**–**G26**, *vide infra*).[42] Notably, the *N*=13 GNR **G7** was built up from a poly(*p*-phenylene ethynylene)(PPE) instead of

typical PPPs, which was advantageous because it is generally easier to obtain high-molecular-weight PPEs than PPPs (Fig. 8). Indeed, the A_2B_2-type Sonogashira polymerisation of **M7a** and **M7b** afforded **P7** with a high M_n=106.5 kDa and $Đ$=1.85 (SEC-MALLS). By utilising the copper-catalysed benzannulation[43] of the internal alkyne unit of **P7** with aldehyde **M7c**, GNR precursor polymer **P7ben** was prepared, and then the following cyclodehydrogenation produced **G7** with the length of 50 nm (based on the molecular weight of **P7**). The optical bandgap of a dispersion of **G7** was observed to be 1.1 eV; however, the solid-state optical bandgap on device was observed to be lower than 0.4 eV, which can relate to the low on–off current ratios (1.8 to 3.1) observed in the device of **G7**.

2.3 *N*=3k+2 Armchair graphene nanoribbons

***N*=5 armchair GNRs.** The width of *N*=5 armchair GNRs is the same as that of naphthalene or perylene. Although oligorylenes have been extensively studied and synthesised in various manners,[44] polyrylenes (*N*=5 armchair GNRs) was not prepared until recently. In 2012, Higashihara, Chen, and Ueda synthesised a polythiophene bearing phenyl groups at the 3-position (**P8**) by the Grignard-metathesis-method (GRIM) polymerisation of **M8a** (Fig. 9). **P8** was then oxidised by 50 equiv $FeCl_3$ to afford GNR **G8** via the oxidative cyclodehydrogenation, which can be considered a sulfur-annulated *N*=5 armchair GNR.[45] Owing to the living chain-growth nature of GRIM, a block copolymer, poly(3-hexylthiophene)(P3HT)-*block*-**G8,** was prepared in the same manner. The optical bandgap (~1.9 eV) and the average hole mobility (1.1 x 10^{-5} $cm^2V^{-1}s^{-1}$) of P3HT-*block*-**G8** (M_n=7.5 kDa, $Đ$=1.29) were similar to those of P3HT homopolymer possibly due to the short **G8** block (the Degree of polymerisation (DP) = < 8).

The successful synthesis of longer *N*=5 armchair GNRs was reported in 2016 by Chalifoux (Fig. 10a).[46] The monomer **M9** was polymerised via the Suzuki–Miyaura coupling to give bis(alkynyl)PPP (**P9**) with M_n= 27.4 kDa and $Đ$=1.4. Then, **P9** was further cyclised by benzannulation under acidic conditions in the absence of any oxidant to afford armchair GNR **G9** with an average estimated length of 35 nm. The optical bandgap of this narrow GNR was measured to be 1.03 eV. In contrast to poorly soluble **G8**, **G9** featured excellent solubility in common organic solvents such as THF and chloroform. Contrary to the recent observation by Wu that cyclopenta-ring-fused oligorylenes have intrinsic high reactivity coming from a diradical character,[47] **G9** was not reported to have specific instability. Above all, the synthetic route to **G9** shows an important alternative of the oxidative cyclodehydrogenation for the graphenisation step.

In 2017, Müllen developed a synthesis of a poly(perylene) (**P10**) with M_n=25 kDa and $Đ$=2.9 via an *AA*-type Yamamoto polymerisation of 3,9/3,10-dibromo-1,6,7,12-tetrakis[*tert*-octylphenoxy]perylene (**M10a/M10a'**) (Fig. 10b). The polyperylene **P10** was converted to *N*=5 armchair GNR **G10** through oxidative cyclodehydrogenation with DDQ and $Sc(OTf)_3$.[48] After the typical polymerisation–graphenisation approach, Müllen further attempted a concise approach to prepare an *N*=5 armchair GNR (**G10**) directly from a perylene monomer, just as surface-assisted synthesis. Tetrabromo-monomer **M10b** was polymerised through the Yamamoto coupling to directly generate **G10**. Although the **G10** prepared by this method was significantly shorter (M_n=4300, $Đ$=2.5), it eliminated the harsh graphenisation step.

***N*=8 armchair GNR.** Crystal topochemical polymerisation was revisited by Rubin in 2017 to synthesise *N*=8 armchair GNRs (Fig. 11a).[49] Crystals of diacetylene monomers containing different side-chains (**M11a–d**) were polymerised under light to give poly(diacetylene)s **P11a–d**, respectively. Heating of the poly(diacetylene)s under an inert atmosphere (500–600 °C) promoted a cascade cyclisation with the polymer backbone, cyclodehydrogenation, and side-chain thermolysis, which quantitatively yielded *N*=8 armchair GNR **G11** with no side-chains.

Very recently, Itami disclosed an innovative way to synthesise *N*=8 armchair GNRs.[50] Annulative π-extension (APEX), which was previously shown for nanographene synthesis,[27, 28] was successfully extended to polymerisation, first affording Fjord-type GNR **G12** in a living chain-growth manner (Fig. 11b). The initiation occurred at the *K*-region (see Fig. 1) of phenanthrene (**Ini1**) reacting with monomer **M12**, and then the chain-propagation continuously occurred at the *K*-regions that are newly-generated by APEX. The molecular weights of **G12a** were controlled up to the monomer-to-initiator ratio of 500 (DP=500), the length of which was calculated to 169 nm. The living chain-growth character also enabled block copolymerisation for a block GNR **G12c**. Furthermore, the cyclodehydrogenation successfully converted **G12a** to *N*=8 armchair GNR **G12b** (Fig. 11c). The optical bandgap of the resulting *N*=8 armchair GNR (~1 eV) was observed to be larger than that of the theoretically-predicted pristine *N*=8 armchair GNR (0.42 eV[29]); however, the origin of this discrepancy was unclear.

2.4 Isomeric armchair graphene nanoribbons

***Meta*-armchair GNR.** An uncommon GNR was synthesised by Müllen in 2012 (Fig. 12).[51] An *AA*-type Yamamoto polymerisation of **M13** produced a polyphenylene containing an alternative *meta*-*para* connectivity (**P13**) with M_n=44 kDa and $Đ$=1.2 (after prep SEC), which, upon treatment with $FeCl_3$, formed a unique armchair-like GNR (**G13**), namely *meta*-armchair GNR. The wide GNR **G13** exhibited the optical bandgap of 1.12 eV, similar to bandgaps of silicon-based semiconductors (1.1 eV).

***Para*-armchair GNR.** In 2015, Feng and Müllen synthesised a new GNR that is isomeric to *meta*-armchair GNRs, which is named as *para*-armchair GNRs. Using the A_2B_2-type Suzuki–Miyaura polymerisation, PPP **P14a** (M_n=4060, $Đ$=1.7) was afforded in 73% yield, and the following cyclodehydrogenation with $FeCl_3$ afforded a *para*-armchair GNR **G14a**, which showed the optical bandgap of 1.44 eV (Fig. 13a).[52]

Mai and Feng discovered that an *AA*-type Yamamoto polymerisation afforded a similar PPP **P14b** with a higher molecular weight (M_n=82.1 kDa, $Đ$=1.1 after prep SEC fractionation),[53] which was graphenised **P14b** to give *para*-armchair GNRs **G14b** (Fig. 13b).[54] The ester side-chains of **G14b** can be hydrolysed under a basic condition and functionalised with poly(ethylene glycol)s (PEGs) via EDC coupling. The post-functionalised GNR **G14PEG** (46% PEG grafting) was well-dispersed in THF (1 mg/mL) as well as in water (0.2 mg/mL), owing to the hydrophilic PEG-containing side-chains. The optical bandgap of **G14PEG** in water (1.0 eV) was lower than that in THF (1.3 eV), probably owing to more aggregation of this material in water.[54] In 2018, Cerullo and Mai prepared a similar *para*-armchair GNRs **G15** with bulky side-chains synthesised through a Diels−Alder reaction of anthracenyl units and *N*-hexadecyl maleimide (Fig. 13c).[55] The bulky side groups on **G15** effectively suppressed the aggregation of GNR chains, exhibiting excellent dispersibility (5 mg/mL) in many organic solvents such as THF, DCM, and toluene. Dilute dispersions in THF consisted mainly of nonaggregated ribbons, which displayed the optical bandgap of a single GNR **G15** (1.69 eV) without contamination of light-scattering signals by GNR aggregates.[56, 57] In addition, this GNR showed near-IR emission with a high quantum yield (9.1%) and a long lifetime (8.7 ns).

Later in 2019, Mai functionalised **G14c** with benzyl ether-type dendrons, instead of PEG, via DCC coupling (Fig. 14).[58] The dendronised GNRs, **G14Den0**, **G14Den1**, and **G14Den2** (59%−68% dendron grafting), were more well-dispersed in THF (1.5−3 mg/mL) than **G14PEG**. Interestingly, one-dimensional self-assembled structures of **G14Den0** (long nanowires), **G14Den1** (long helices) and **G14Den2** (short nanofibers) were observed in solution. **G14Den2** showed a similar optical bandgap (1.3 eV) to **G14PEG** in THF, whereas more ordered aggregates of **G14Den0** and **G14Den1** in THF showed red-shifted absorptions.

3. Graphene nanoribbons with non-armchair edges

3.1 Zigzag graphene nanoribbons

The successful bottom-up synthesis of zigzag GNRs has been demonstrated by Müllen and Fasel through surface-assisted protocols.[59] However, liquid-phase synthesis of zigzag GNRs has not been reported yet.

3.2 Cove/Cove-type graphene nanoribbons

Cove GNRs are zigzag GNRs with periodic carbon atom vacancies on both edges (Fig. 1).[60] A pristine cove GNR was first synthesised by Feng and Müllen (Fig. 15a).[61] In this case, oligomers were produced in solution via Ullmann coupling followed by DDQ oxidation, whereas the corresponding cove GNR was prepared on a metal surface.

On the other hand, GNRs with cove-like edges have also been successfully prepared in solution. In 2014, based upon their previous protocols for synthesis of nanographenes,[62-64] the same research group developed an elegant metal-free bottom-up approach to synthesise cove-type GNRs, where the *AB*-type Diels–Alder reaction between cyclopentadienones and alkynes was employed (Fig. 15b).[6] The polymerisation initially produced precursor polymer **P16** with a broad molecular weight dispersity (M_n=41 kDa, $Đ$=13), but SEC fractionation successfully isolated **P16** with high-molecular-weight portions (M_n=340 kDa, $Đ$=1.9), which was subjected to the cyclodehydrogenation conditions to give long GNR **G16** (>200 nm). Cove-type edges containing bulky side-chains on their peripheral positions effectively alleviated aggregations of long **G16**, thus displaying decent dispersibility in common organic solvents such as THF and chlorobenzene. The optical bandgap of **G16** was measured to be 1.88 eV, which is relatively high compared to bandgaps of armchair GNRs with similar widths. In addition, **G16** featured a high carrier mobility of 150—15,000 $cm^2V^{-1}s^{-1}$. The same protocol has also been employed to synthesise a wider cove-type GNR **G16W**, which possessed lower bandgap than **G16** (1.24 vs 1.88 eV) (Fig. 15c).[65]

Apart from the lateral extension, Müllen and Narita presented a different approach for compressing bandgaps of cove-type GNRs (Fig. 15d and e). In 2018, they achieved the synthesis of planar **G16a** and nonplanar **G16b** from the precursor polymers prepared via the Diels–Alder polymerisation, **P16a** (M_n=83 kDa, $Đ$=1.5 after prep SEC) and **P16b** (M_n=68 kDa, $Đ$=1.8 after prep SEC).[66] With the same aromatic core structure, the peripheral benzo-rings of **G16b** were distorted by ca. 24° from planarity, while **G16a** was flat. The optical bandgap of **G16b** (1.25 eV) was 0.18 eV lower than that of **G16a** (1.43 eV), which is associated with a lower conduction band. This was likely due to that the structural distortion at the edge alleviates the aggregation of cove GNRs. This approach is free from the drawback of the lateral extension strategy — the trade-off between the bandgap compression and processability.

A divergent protocol for edge functionalisation of cove-type GNRs was also developed by Müllen and Narita in 2017 (Fig. 16).[67] Bromo-functionalised **P17** (M_n=102 kDa, $Đ$=2.7 after purification), prepared from mono-bromo-functionalised monomer **M17** via the Diels–Alder polymerisation, was diversified by introduction of perylene monoamide (PMI), naphthalene monoamide (NMI) and anthraquinone (AQ) units at the peripheral positions of **P17** by the Suzuki–Miyaura coupling. The consecutive cyclodehydrogenation of **P17a-c** with $FeCl_3$ yielded edge-functionalised **G17a-c**. In 2018, Bogani disclosed a cove-type GNR functionalised with spin-bearing radical groups (Fig. 16).[68] After graphenisation of **P17**, nitronyl nitroxide radicals as magnetic injectors was introduced onto **G17** via the palladium-catalysed cross-coupling, affording a magnetically functionalised **G17rad**.[59] Spin injection from the nitronyl nitroxide radicals into the GNR core induced magnetic edge states of GNRs, which opens a door for the potential spintronic applications of GNRs.

3.3 Chevron-type graphene nanoribbons

Sinitskii reported a gram-scale synthetic approach for chevron-type GNRs **G18** (Fig. 17). An *AA*-type Yamamoto polymerisation was used to construct the GNR precursor **P18**, followed by oxidative cyclodehydrogenation with $FeCl_3$.[69] It is noted that **G18** featured GNRs with no side-chains in stark contrast to the general GNRs with bulky side-chains as solubilising groups. The absence of side-chains facilitated scanning probe microscopic/spectroscopic analyses (e.g. STM, STS, AFM), but made characterisation of GNR precursors (e.g. NMR, SEC) and liquid-phase processes of the GNRs challenging. The limitation of processability was partially resolved by efforts of Sinitskii and Lyding, respectively. Sinitskii developed a new fabrication method that makes films of single-GNR thick (2 nm), which exploits the high dispersibility of **G18** in chlorosulfonic acid and water-air interfacial self-assembly.[70] On the other hand, Lyding reported a clean deposition method of **G18** onto hydrogen-terminated Si(100) surface.[71]

The edge structures of chevron GNRs are difficult to define though large portions of them are armchair-edged. The optical bandgap of **G18** was 1.3 eV, which is similar to that of *N*=6 or *N*=9 armchair GNR (see Figs. 3 and 6). Later, a laterally extended chevron-type GNR **G21** was also prepared by Sinitski in a similar approach, which found application as a gas sensor for methanol and ethanol.[72]

In addition, nitrogen-doped chevron-type GNRs, **G19** and **G20**, were synthesised analogously by Sinitskii and Sutter.[73, 74] The nitrogen doping significantly affects inter-GNR interactions (e.g. N···H–C hydrogen bondings, van der Waals interactions, and π–π interactions at the basal planes of **G19** and **G20**), which consequently generated the hierarchical self-assembly of N-doped GNRs into ordered structures.

In 2019, Fischer developed a creative route to a chevron-type GNR. Ring-opening alkyne metathesis polymerisation (ROAMP) of strained cyclic diynes (**M22a**) afforded **P22a** in a controlled chain-growth manner. The molecular weights of **P22a** were controlled up to the monomer-to-initiator ratio of 40 (DP=40), the length of which was calculated to 68 nm. The alkynes of **P22a** were quantitatively converted to phenylene units by Diels–Alder reactions with cyclopentadienone **M22b**, and the resulting GNR precursor polymer **P22b** was subsequently cyclodehydrogenated to give a chevron GNR **G22**.[75]

3.4 Kinked graphene nanoribbons

Relatively flexible kinked GNRs were designed to address the solubility issue of GNRs derived from rigid PPPs (e.g. **G1b** and **G2**). In 2011, Müllen synthesized soluble kinked GNRs **G23** (M_n=20 kDa) via the Suzuki–Miyaura polymerisation followed by oxidative cyclodehydrogenation (Fig. 18).[76]

The lateral extension of kinked GNRs was achieved, by Jo in 2013, where naphthalene diboronic ester **M24a** or anthracene diboronic ester **M24b** was polymerised instead of **M6a**. While the cyclodehydrogenation from **P24** to **G24** was successful, the incomplete graphenisation was observed in the case of **G25** (78%) and **G26** (75%). Thin-film transistors (TFTs) were fabricated with these kinked GNRs, which displayed ambipolar transport behaviour, just as the device made of **G7** (*vide supra*). In particular, TFT made of **G26** exhibited better performance (μ_{hole} = 3.25 x 10^{-2} $cm^2V^{-1}s^{-1}$ and $\mu_{electron}$ = 7.11 x 10^{-3} $cm^2V^{-1}s^{-1}$) than those made of **G24** and **G25** due to better π–π stacking.[42]

Switching the 1,2-dibromobenzene to a pyrazine-derived monomer (**M27**), the Suzuki–Miyaura polymerisation followed by cyclodehydrogenation (>95% efficiency) afforded nitrogen-doped **G27** (M_n=16.1 kDa, $Đ$=1.49) (Fig. 18). In addition, the degree of nitrogen doping can be simply controlled through a copolymerisation process by changing the feed ratio of **M27** (pyrazine) to **M23L** (benzene) (e.g. **G28**). The electron mobility of **G27** (0.102 $cm^2V^{-1}s^{-1}$) was two orders of magnitude higher than that of **G25** (4.57 x 10^{-3} $cm^2V^{-1}s^{-1}$), which showed the nitrogen doping modified the electronic transport behaviour from ambipolar to n-type.[77]

3.5 Fjord-type graphene nanoribbons

A photochemical cyclodehydrochlorination (CDHC) reaction was first employed for the GNR synthesis by Morin. This reaction is not only a relatively mild alternative to the commonly used oxidative methods in the graphenisation step but also a nice way to construct fjord-type edge structures.

In 2017, Morin developed synthesis of a helically coiled GNR **G29** from a polychlorinated poly(*m*-phenylene) **P29** via CDHC (Fig. 20).[78] Given that one helical pitch consists of six monomeric units, the DP value of 32 represents ca. 5 helical pitches. Another structural feature of **G29** was the fjord-type inner edge. **G29** showed a large optical band gap (2.15 eV) compared to other GNRs and is highly emissive both in solution and the solid state. It is unclear whether these characters resulted from the fjord edge and/or the helical structure.

Later, Morin also reported an approach to prepare thiophene-edged graphene nanoribbons (**G30** and **G31**) from thiophene-containing polychlorinated PPPs (**P31** and **P31**) via CDHC.[79] The substitution positions of the thiophenyl groups on the PPPs played a critical role in the electronic properties of the GNR. For example, the optical bandgap of **G31** (2.61 eV) is 0.3 eV lower than that of **G30** (2.91 eV). In addition, **G29** and **G30** featured unsymmetrical edge structures, similar to the *N*=6 armchair GNRs (Fig. 6). As aforementioned in the previous section (*vide supra*, Fig. 11), the APEX polymerisation of **M11** directly afforded fjord GNR **G11** (M_n=150 kDa, $Đ$=1.22), which showed the optical bandgap to be >2.5 eV.

4. Conclusions and outlook

Since 2000, great advances in liquid-phase bottom-up syntheses have been achieved, which provide access to GNRs with a variety of structures in laboratories, as covered in this review (Fig. 21). Yet, this young research field still demands more important breakthroughs to meet high expectations for (industrial) practical applications.

First, liquid-phase bottom-up approaches hold great potentials for edge functionalisation. The functional groups on

the GNR edges could allow for manipulating and fine-tuning properties of the materials, including band gap engineering, water solubility and binding ability of metal ions. Currently, the graphenisation step in most syntheses requires strong acids, strong oxidants, and/or high temperatures, which would limit the types of functional groups to be introduced due to chemical compatibilities. While a few recent efforts, e.g. alkyne benzannulation and cyclodehydrohalogenation, have alleviated the constraint to some extent, general and milder graphenisation approaches (e.g. no acid at r.t.) are still highly sought.

Another ongoing challenge is to confirm the structural integrity of GNRs, that is, to rapidly identify defects. Common solid-state spectroscopic analyses (solid-state NMR, MALDI, IR, Raman, XPS, etc.) are helpful and complementary to each other, but still disputable. Interdisciplinary efforts would be needed to discover conclusive protocols for GNR characterisation.

Self-assembly of GNRs is another ongoing interest. Recent progress in living chain-growth polymerisations for GNRs enables the length control of GNRs as well as block copolymer synthesis, which opens up the possibility of systemic preparation of high-ordered nanostructures from block co-GNRs. In addition, the inter-GNR interactions enabled by nitrogen-doped GNRs created new opportunities for hierarchical assembly through non-covalent bonds.

Finally, targeted as the next-generation semiconductors, GNRs ought to be produced cost effectively and subjected to large scales. While gram-scale synthesis of GNRs has been achieved in liquid phase to date, further scale-up could be hampered by the overall synthetic efficiency. This in turn calls for better design and more streamlined syntheses of GNR monomers, as well as more selective, efficient and controlled polymerisation and graphenisation methods.

Conflicts of interest

There are no conflicts to declare.

Acknowledgements

University of Chicago and NSF (CHE 1707399) are acknowledged for research support.

References

1. A. Facchetti, *Mater. Today*, 2007, **10**, 28-37.
2. H. Klauk, *Organic electronics: materials, manufacturing, and applications*, John Wiley & Sons, 2006.
3. T. B. Singh and N. S. Sariciftci, *Annu. Rev. Mater. Res.*, 2006, **36**, 199-230.
4. X. Guo, M. Baumgarten and K. Müllen, *Prog. Polym. Sci.*, 2013, **38**, 1832-1908.
5. J. Wang, R. Zhao, M. Yang, Z. Liu and Z. Liu, *J. Chem. Phys.*, 2013, **138**, 084701.
6. A. Narita, X. Feng, Y. Hernandez, S. A. Jensen, M. Bonn, H. Yang, I. A. Verzhbitskiy, C. Casiraghi, M. R. Hansen, A. H. R. Koch, G. Fytas, O. Ivasenko, B. Li, K. S. Mali, T. Balandina, S. Mahesh, S. De Feyter and K. Müllen, *Nat. Chem.*, 2014, **6**, 126-132.
7. S. Dutta and S. K. Pati, *J. Mater. Chem.*, 2010, **20**, 8207-8223.
8. Y.-W. Son, M. L. Cohen and S. G. Louie, *Phys. Rev. Lett.*, 2006, **97**, 216803.
9. O. V. Yazyev, *Acc. Chem. Res.*, 2013, **46**, 2319-2328.
10. A. Celis, M. N. Nair, A. Taleb-Ibrahimi, E. H. Conrad, C. Berger, W. A. de Heer and A. Tejeda, *J. Phys. D Appl. Phys.*, 2016, **49**, 143001.
11. L. Ma, J. Wang and F. Ding, *ChemPhysChem*, 2013, **14**, 47-54.
12. A. Narita, Z. Chen, Q. Chen and K. Mullen, *Chem. Sci.*, 2019, **10**, 964-975.
13. A. Narita, X. Feng and K. Mullen, *Chem. Rec.*, 2015, **15**, 295-309.
14. M. Shekhirev and A. Sinitskii, *Phys. Sci. Rev.*, 2017, **2**, 12807-12821.
15. L. Talirz, P. Ruffieux and R. Fasel, *Adv. Mater.*, 2016, **28**, 6222-6231.
16. Y. C. Teo, H. W. H. Lai and Y. Xia, *Chem. Eur. J.*, 2017, **23**, 14101-14112.
17. Y. Segawa, H. Ito and K. Itami, *Nat. Rev. Mater.*, 2016, **1**, 15002.
18. X.-Y. Wang, A. Narita and K. Müllen, *Nat. Rev. Chem.*, 2017, **2**, 0100.
19. W. Niu, J. Liu, Y. Mai, K. Müllen and X. Feng, *Trends Chem.*, 2019, **1**, 549-558.
20. J. F. Morin, A. Jolly, D. Miao and M. Daigle, *Angew. Chem. Int. Ed.*, 2019, DOI: 10.1002/anie.201906379.
21. A. D. Senese and W. A. Chalifoux, *Molecules*, 2019, **24**, 118.
22. K. Müllen, *ACS Nano*, 2014, **8**, 6531-6541.
23. L. Chen, Y. Hernandez, X. Feng and K. Müllen, *Angew. Chem. Int. Ed.*, 2012, **51**, 7640-7654.
24. A. Narita, X.-Y. Wang, X. Feng and K. Müllen, *Chem. Soc. Rev.*, 2015, **44**, 6616-6643.
25. X.-Y. Wang, X. Yao and K. Müllen, *Sci. China Chem.*, 2019, **9**, 1099-1144.
26. X. Feng, W. Pisula and K. Müllen, *Pure Appl. Chem.*, 2009, **81**, 2203-2224.
27. H. Ito, Y. Segawa, K. Murakami and K. Itami, *J. Am. Chem. Soc.*, 2018, **141**, 3-10.
28. H. Ito, K. Ozaki and K. Itami, *Angew. Chem. Int. Ed.*, 2017, **56**, 11144-11164.
29. D. Prezzi, D. Varsano, A. Ruini, A. Marini and E. Molinari, *Phys. Rev. B*, 2008, **77**, 041404.
30. H. Raza and E. C. Kan, *Phys. Rev. B*, 2008, **77**, 245434.
31. S. Osella, A. Narita, M. G. Schwab, Y. Hernandez, X. Feng, K. Müllen and D. Beljonne, *ACS Nano*, 2012, **6**, 5539-5548.
32. X. Zhu and H. Su, *J. Phys. Chem. A*, 2011, **115**, 11998-12003.
33. Z. B. Shifrina, M. S. Averina, A. L. Rusanov, M. Wagner and K. Müllen, *Macromolecules*, 2000, **33**, 3525-3529.
34. J. Wu, L. Gherghel, M. D. Watson, J. Li, Z. Wang, C. D. Simpson, U. Kolb and K. Müllen, *Macromolecules*, 2003, **36**, 7082-7089.
35. X. Yang, X. Dou, A. Rouhanipour, L. Zhi, H. J. Räder and K. Müllen, *J. Am. Chem. Soc.*, 2008, **130**, 4216-4217.
36. G. Li, K.-Y. Yoon, X. Zhong, X. Zhu and G. Dong, *Chem. Eur. J.*, 2016, **22**, 9116-9120.
37. O. Hod, J. E. Peralta and G. E. Scuseria, *Phys. Rev. B*, 2007, **76**, 233401.
38. M. El Gemayel, A. Narita, L. F. Dössel, R. S. Sundaram, A. Kiersnowski, W. Pisula, M. R. Hansen, A. C. Ferrari, E. Orgiu, X. Feng, K. Müllen and P. Samorì, *Nanoscale*, 2014, **6**, 6301-6314.

39. R. S. Jordan, Y. Wang, R. D. McCurdy, M. T. Yeung, K. L. Marsh, S. I. Khan, R. B. Kaner and Y. Rubin, *Chem*, 2016, **1**, 78-90.
40. G. Li, K.-Y. Yoon, X. Zhong, J. Wang, R. Zhang, J. R. Guest, J. Wen, X.-Y. Zhu and G. Dong, *Nat. Commun.*, 2018, **9**, 1687.
41. J. Gao, F. J. Uribe-Romo, J. D. Saathoff, H. Arslan, C. R. Crick, S. J. Hein, B. Itin, P. Clancy, W. R. Dichtel and Y.-L. Loo, *ACS Nano*, 2016, **10**, 4847-4856.
42. K. T. Kim, J. W. Jung and W. H. Jo, *Carbon*, 2013, **63**, 202-209.
43. S. J. Hein, D. Lehnherr, H. Arslan, F. J Uribe-Romo and W. R. Dichtel, *Acc. Chem. Res.*, 2017, **50**, 2776-2788.
44. J. T. Markiewicz and F. Wudl, *ACS Appl. Mater. Interfaces*, 2015, **7**, 28063-28085.
45. A. Takahashi, C.-J. Lin, K. Ohshimizu, T. Higashihara, W.-C. Chen and M. Ueda, *Polym. Chem.*, 2012, **3**, 479-485.
46. W. Yang, A. Lucotti, M. Tommasini and W. A. Chalifoux, *J. Am. Chem. Soc.*, 2016, **138**, 9137-9144.
47. W. Zeng, H. Phan, T. S. Herng, T. Y. Gopalakrishna, N. Aratani, Z. Zeng, H. Yamada, J. Ding and J. Wu, *Chem*, 2017, **2**, 81-92.
48. D. Jänsch, I. Ivanov, Y. Zagranyarski, I. Duznovic, M. Baumgarten, D. Turchinovich, C. Li, M. Bonn and K. Müllen, *Chem. Eur. J.*, 2017, **23**, 4870-4875.
49. R. S. Jordan, Y. L. Li, C.-W. Lin, R. D. McCurdy, J. B. Lin, J. L. Brosmer, K. L. Marsh, S. I. Khan, K. N. Houk, R. B. Kaner and Y. Rubin, *J. Am. Chem. Soc.*, 2017, **139**, 15878-15890.
50. Y. Yano, N. Mitoma, K. Matsushima, F. Wang, K. Matsui, A. Takakura, Y. Miyauchi, H. Ito and K. Itami, *Nature*, 2019, **20**, 387-392.
51. M. G. Schwab, A. Narita, Y. Hernandez, T. Balandina, K. S. Mali, S. De Feyter, X. Feng and K. Müllen, *J. Am. Chem. Soc.*, 2012, **134**, 18169-18172.
52. M. G. Schwab, A. Narita, S. Osella, Y. Hu, A. Maghsoumi, A. Mavrinsky, W. Pisula, C. Castiglioni, M. Tommasini, D. Beljonne, X. Feng and K. Müllen, *Chem. Asian J.*, 2015, **10**, 2134-2138.
53. Y. Huang, Y. Mai, X. Yang, U. Beser, J. Liu, F. Zhang, D. Yan, K. Müllen and X. Feng, *J. Am. Chem. Soc.*, 2015, **137**, 11602-11605.
54. Y. Huang, Y. Mai, U. Beser, J. Teyssandier, G. Velpula, H. van Gorp, L. A. Straasø, M. R. Hansen, D. Rizzo, C. Casiraghi, R. Yang, G. Zhang, D. Wu, F. Zhang, D. Yan, S. De Feyter, K. Müllen and X. Feng, *J. Am. Chem. Soc.*, 2016, **138**, 10136-10139.
55. Y. Huang, F. Xu, L. Ganzer, F. V. A. Camargo, T. Nagahara, J. Teyssandier, H. van Gorp, K. Basse, L. A. Straasø, V. Nagyte, C. Casiraghi, M. R. Hansen, S. De Feyter, D. Yan, K. Müllen, X. Feng, G. Cerullo and Y. Mai, *J. Am. Chem. Soc.*, 2018, **140**, 10416-10420.
56. L. Dong, G. Shang, J. Shi, J. Zhi, B. Tong and Y. Dong, *J. Phys. Chem. C*, 2017, **121**, 11658-11664.
57. K.-Y. Yoon, Y. Xue and G. Dong, *Macromolecules*, 2019, **52**, 1663-1670.
58. F. Xu, C. Yu, A. Tries, H. Zhang, M. Kläui, K. Basse, M. R. Hansen, N. Bilbao, M. Bonn, H. I. Wang and Y. Mai, *J. Am. Chem. Soc.*, 2019, **141**, 10972-10977.
59. P. Ruffieux, S. Wang, B. Yang, C. Sanchez-Sanchez, J. Liu, T. Dienel, L. Talirz, P. Shinde, C. A. Pignedoli, D. Passerone, T. Dumslaff, X. Feng, K. Müllen and R. Fasel, *Nature*, 2016, **531**, 489-492.
60. Y.-L. Lee, F. Zhao, T. Cao, J. Ihm and S. G. Louie, *Nano Lett.*, 2018, **18**, 7247-7253.
61. J. Liu, B.-W. Li, Y.-Z. Tan, A. Giannakopoulos, C. Sanchez-Sanchez, D. Beljonne, P. Ruffieux, R. Fasel, X. Feng and K. Müllen, *J. Am. Chem. Soc.*, 2015, **137**, 6097-6103.
62. D. Wasserfallen, M. Kastler, W. Pisula, W. A. Hofer, Y. Fogel, Z. Wang and K. Müllen, *J. Am. Chem. Soc.*, 2006, **128**, 1334-1339.
63. M. Kastler, J. Schmidt, W. Pisula, D. Sebastiani and K. Müllen, *J. Am. Chem. Soc.*, 2006, **128**, 9526-9534.
64. Y. Fogel, L. Zhi, A. Rouhanipour, D. Andrienko, H. J. Räder and K. Müllen, *Macromolecules*, 2009, **42**, 6878-6884.
65. A. Narita, I. A. Verzhbitskiy, W. Frederickx, K. S. Mali, S. A. Jensen, M. R. Hansen, M. Bonn, S. De Feyter, C. Casiraghi, X. Feng and K. Müllen, *ACS Nano*, 2014, **8**, 11622-11630.
66. Y. Hu, P. Xie, M. De Corato, A. Ruini, S. Zhao, F. Meggendorfer, L. A. Straasø, L. Rondin, P. Simon, J. Li, J. J. Finley, M. R. Hansen, J.-S. Lauret, E. Molinari, X. Feng, J. V. Barth, C.-A. Palma, D. Prezzi, K. Müllen and A. Narita, *J. Am. Chem. Soc.*, 2018, **140**, 7803-7809.
67. A. Keerthi, B. Radha, D. Rizzo, H. Lu, V. Diez Cabanes, I. C.-Y. Hou, D. Beljonne, J. Cornil, C. Casiraghi, M. Baumgarten, K. Müllen and A. Narita, *J. Am. Chem. Soc.*, 2017, **139**, 16454-16457.
68. M. Slota, A. Keerthi, W. K. Myers, E. Tretyakov, M. Baumgarten, A. Ardavan, H. Sadeghi, C. J. Lambert, A. Narita, K. Müllen and L. Bogani, *Nature*, 2018, **557**, 691-695.
69. T. H. Vo, M. Shekhirev, D. A. Kunkel, M. D. Morton, E. Berglund, L. Kong, P. M. Wilson, P. A. Dowben, A. Enders and A. Sinitskii, *Nat. Commun.*, 2014, **5**, 3189.
70. M. Shekhirev, T. H. Vo, M. Mehdi Pour, A. Lipatov, S. Munukutla, J. W. Lyding and A. Sinitskii, *ACS Appl. Mater. Interfaces*, 2016, **9**, 693-700.
71. A. Radocea, T. Sun, T. H. Vo, A. Sinitskii, N. R. Aluru and J. W. Lyding, *Nano Lett.*, 2016, **17**, 170-178.
72. M. M. Pour, A. Lashkov, A. Radocea, X. Liu, T. Sun, A. Lipatov, R. A. Korlacki, M. Shekhirev, N. R. Aluru, J. W. Lyding, V. Sysoev and A. Sinitskii, *Nat. Commun.*, 2017, **8**, 820.
73. T. H. Vo, M. Shekhirev, D. A. Kunkel, F. Orange, M. J. F. Guinel, A. Enders and A. Sinitskii, *Chem. Commun.*, 2014, **50**, 4172-4174.
74. T. H. Vo, U. G. E. Perera, M. Shekhirev, M. Mehdi Pour, D. A. Kunkel, H. Lu, A. Gruverman, E. Sutter, M. Cotlet, D. Nykypanchuk, P. Zahl, A. Enders, A. Sinitskii and P. Sutter, *Nano Lett.*, 2015, **15**, 5770-5777.
75. S. von Kugelgen, I. Piskun, J. H. Griffin, C. T. Eckdahl, N. N. Jarenwattananon and F. R. Fischer, *J. Am. Chem. Soc.*, 2019, **141**, 11050-11058.
76. L. Dössel, L. Gherghel, X. Feng and K. Müllen, *Angew. Chem. Int. Ed.*, 2011, **50**, 2540-2543.
77. K. T. Kim, J. W. Lee and W. H. Jo, *Macromol. Chem. Phys*, 2013, **214**, 2768-2773.
78. M. Daigle, D. Miao, A. Lucotti, M. Tommasini and J.-F. Morin, *Angew. Chem. Int. Ed.*, 2017, **56**, 6213-6217.
79. D. Miao, M. Daigle, A. Lucotti, J. Boismenu-Lavoie, M. Tommasini and J.-F. Morin, *Angew. Chem. Int. Ed.*, 2018, **57**, 3588-3592.

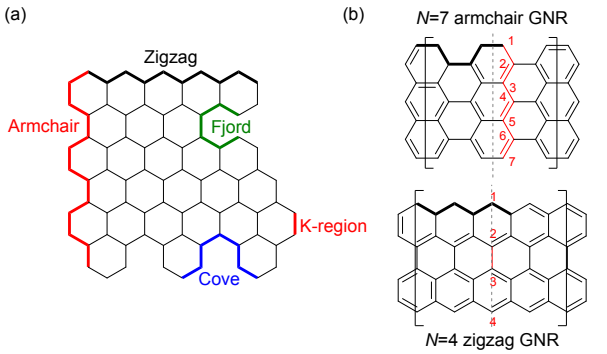

Fig. 1 (a) Terminologies of GNR edges. (b) Examples of the width naming. *N*: the number of rows of atoms forming the ribbon width.

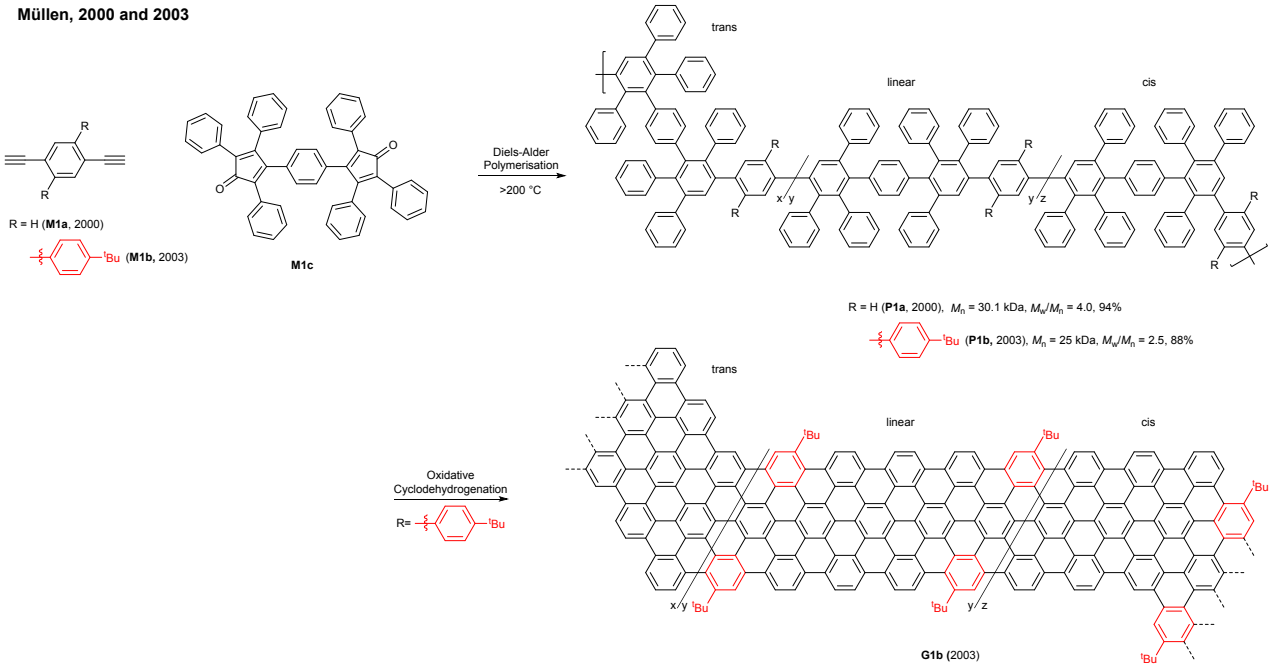

Fig. 2 Synthesis of kinked *N*=9 armchair GNR.

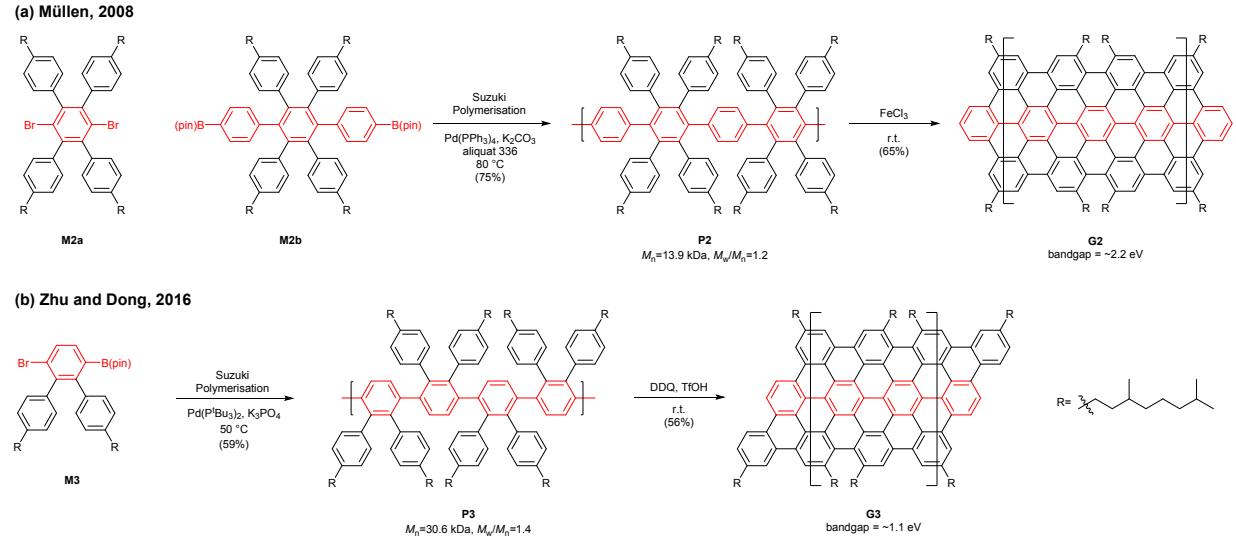

Fig. 3 Synthesis of (linear) *N*=9 armchair GNRs.

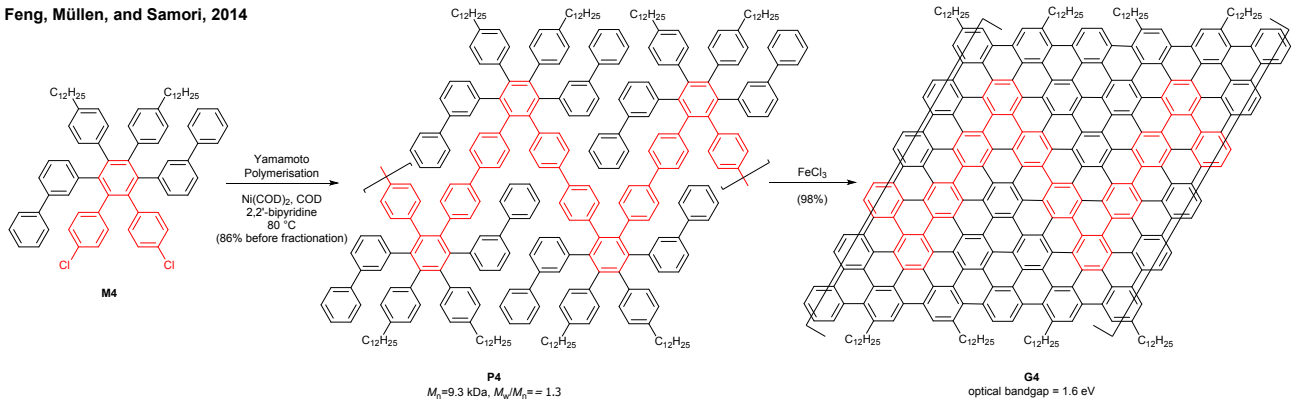

Fig. 4 Synthesis of *N*=18 armchair GNRs.

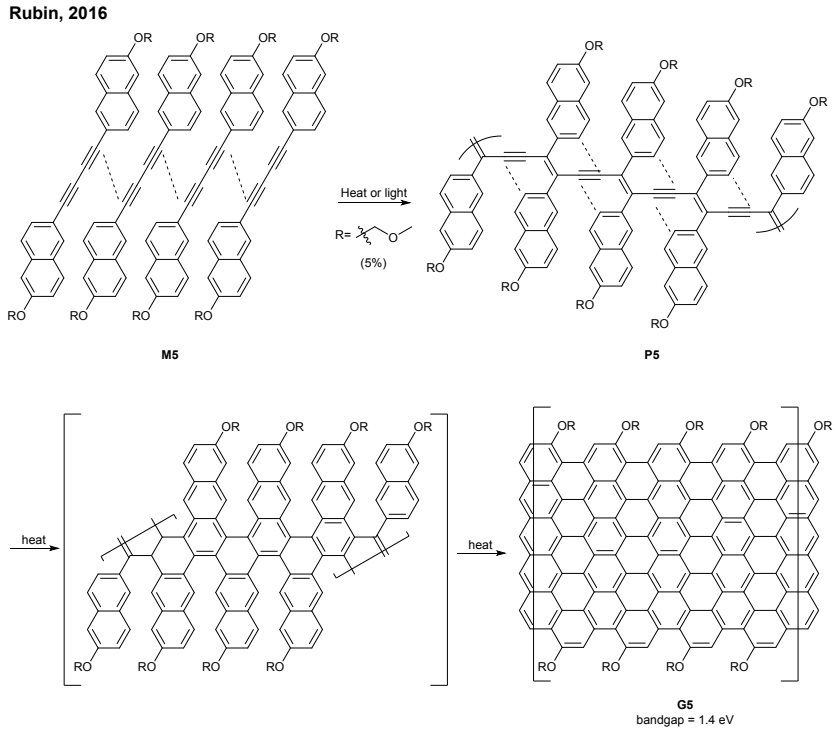

Fig. 5 Synthesis of a *N*=12 armchair GNR.

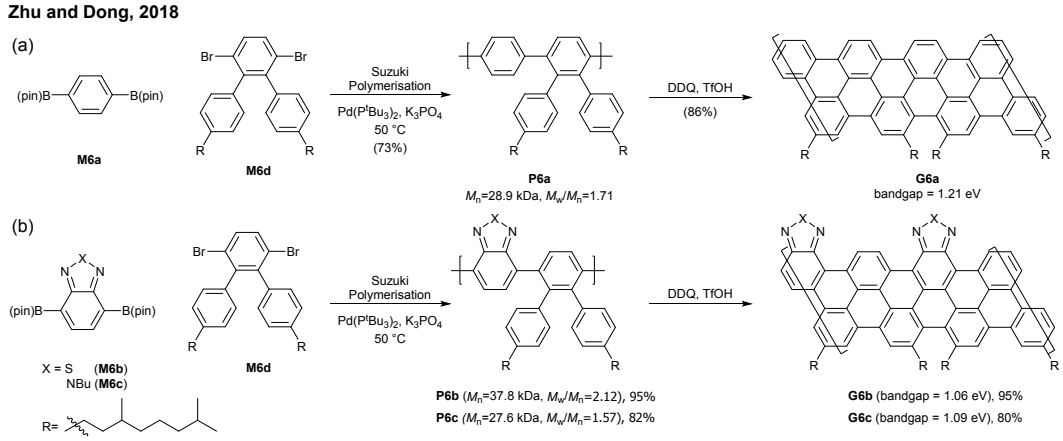

Fig. 6 Synthesis of *N*=6 armchair GNRs.

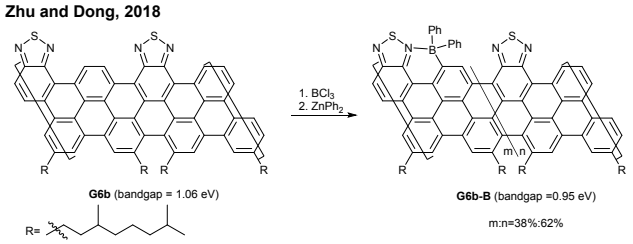

Fig.7 Post-functionalisation of the *N*=6 armchair GNR bearing heterocycles.

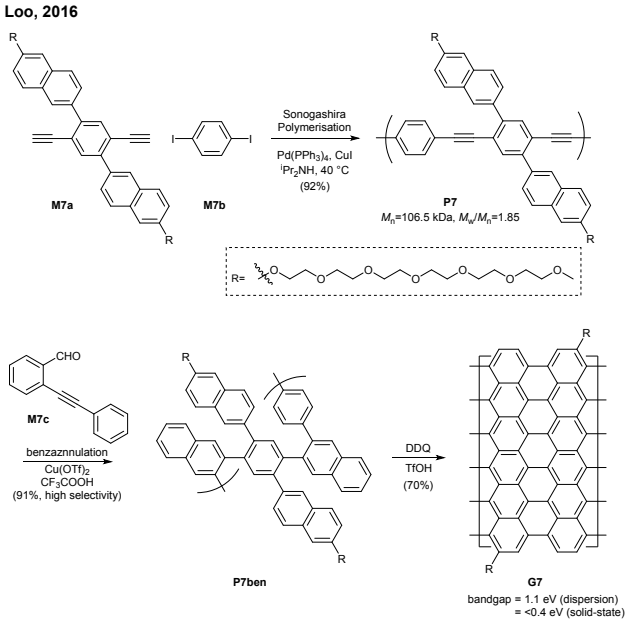

Fig. 8 Synthesis of a *N*=13 armchair GNR.

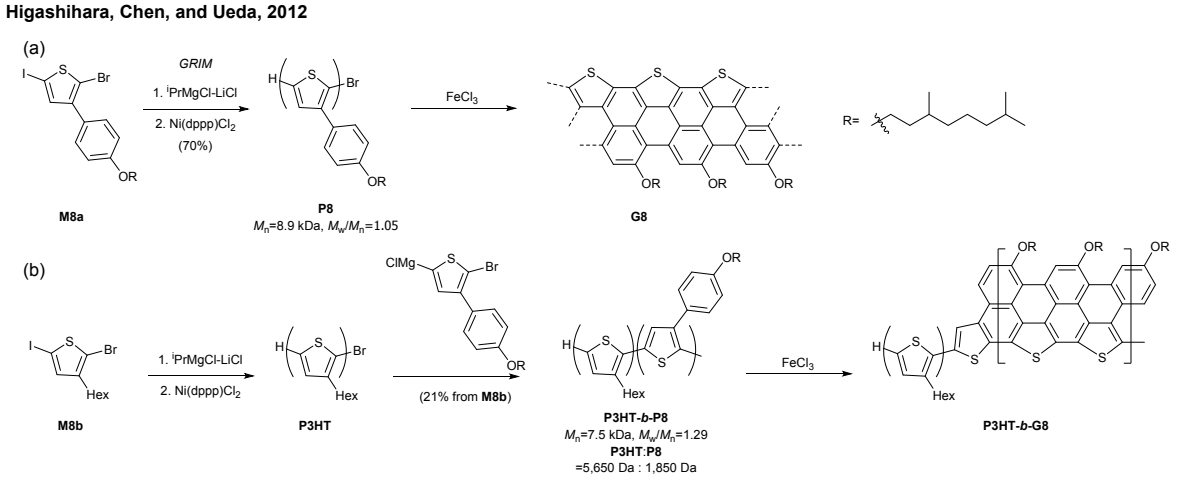

Fig. 9 (a) Synthesis of a S-annulated *N*=5 armchair GNR and (b) a block copolymer containing S-annulated *N*=5 armchair GNRs.

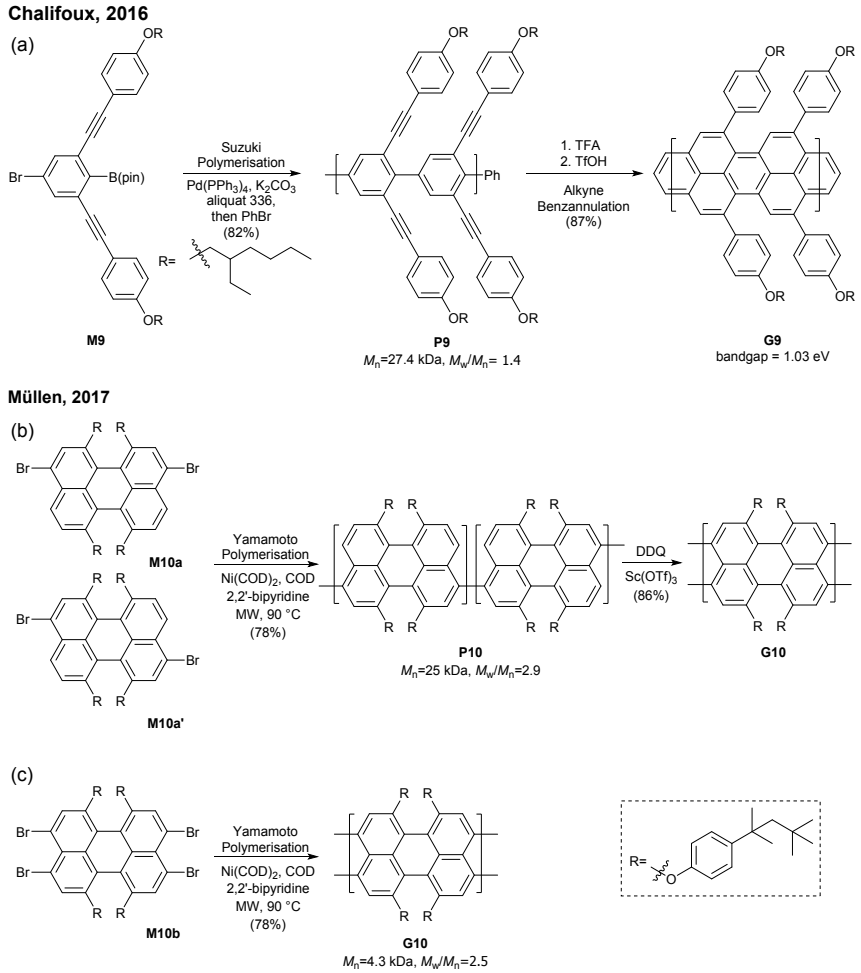

Fig. 10 Synthesis of *N*=5 armchair GNRs.

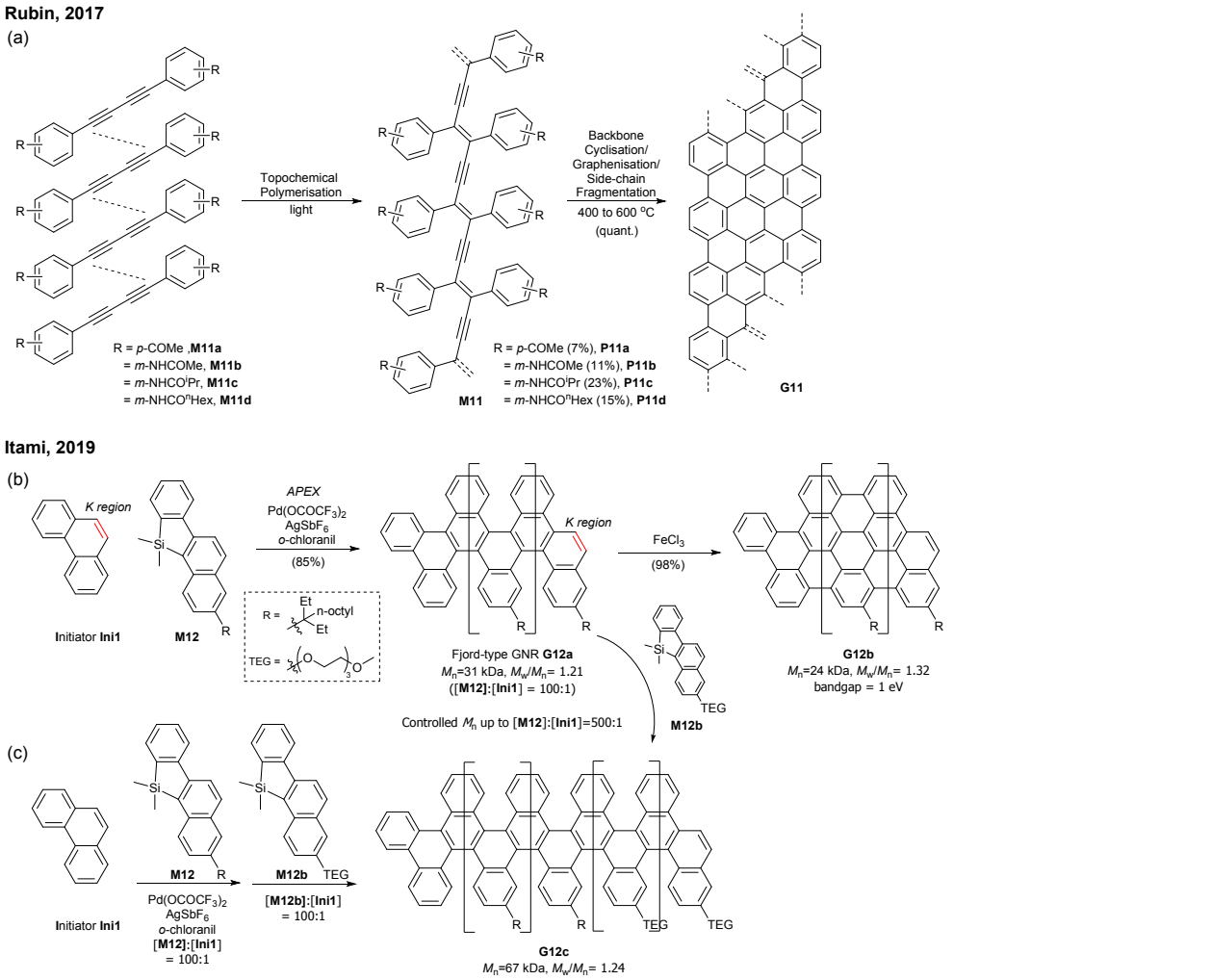

Fig. 11 Synthesis of *N*=8 armchair GNRs.

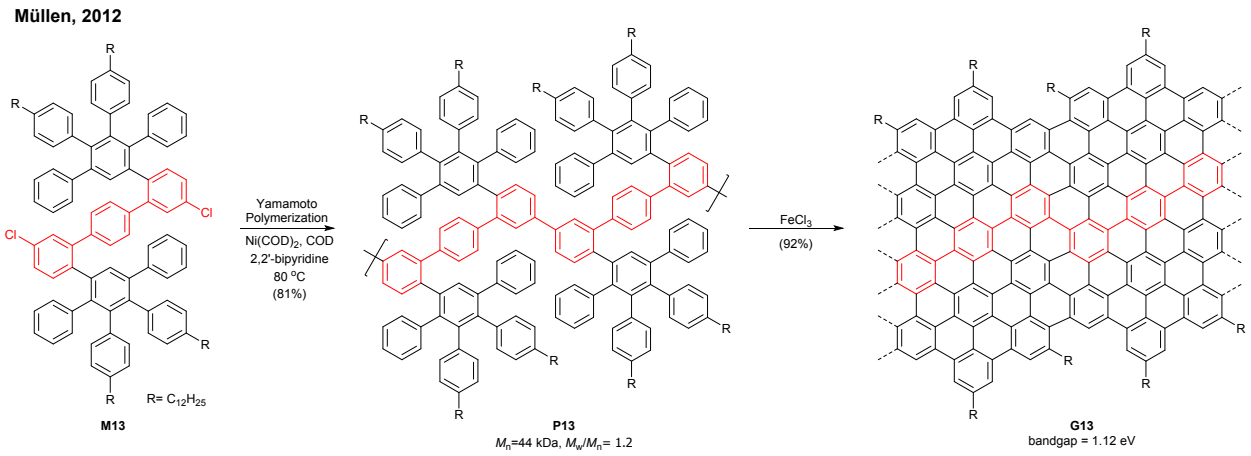

Fig. 12 Synthesis of a *meta*-armchair GNR.

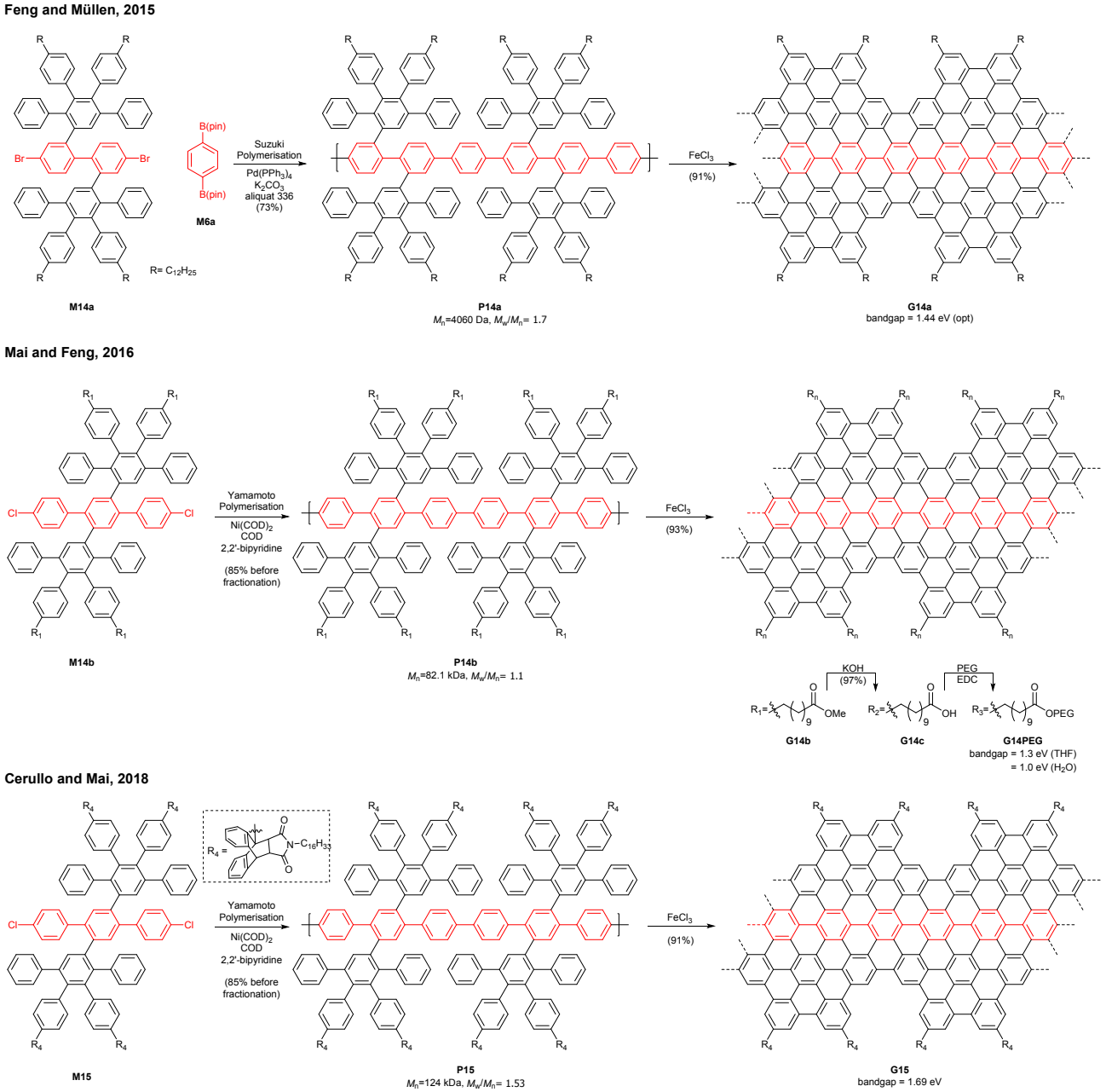

Fig. 13 Synthesis of *para*-armchair GNRs.

Mai, 2019

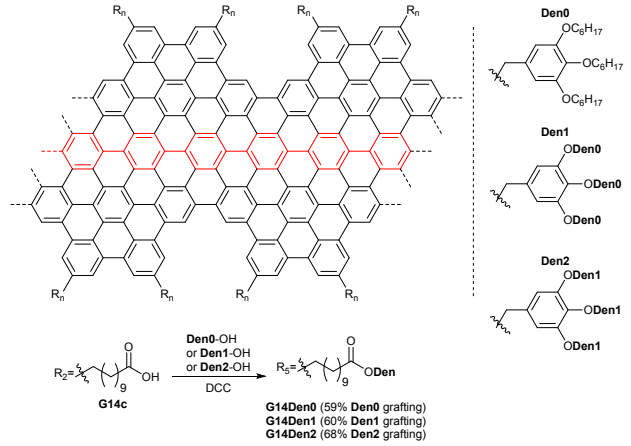

Fig. 14 Synthesis of the dendronised GNRs with *para*-armchair edges.

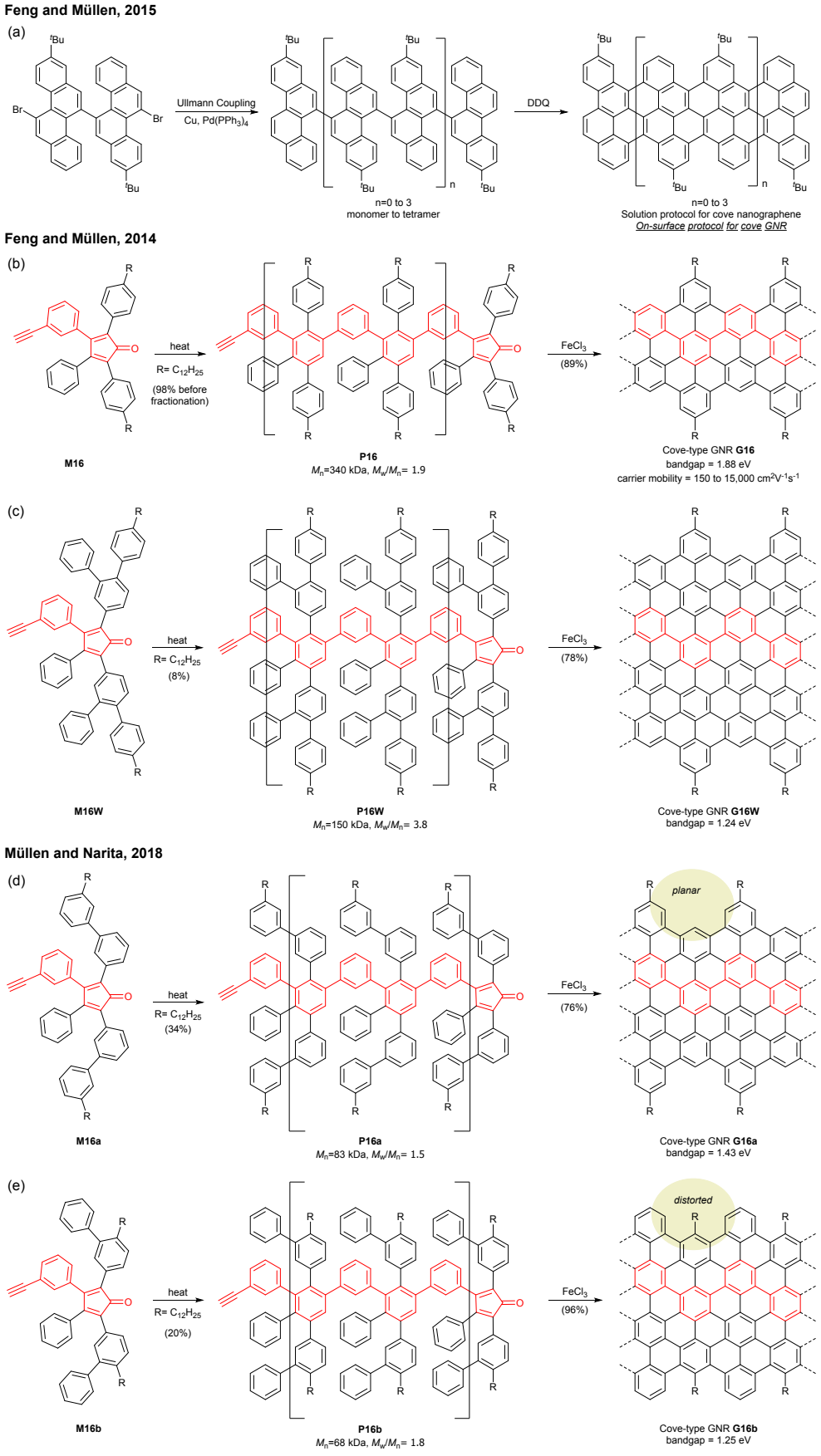

Fig. 15 Synthesis of cove-type GNRs.

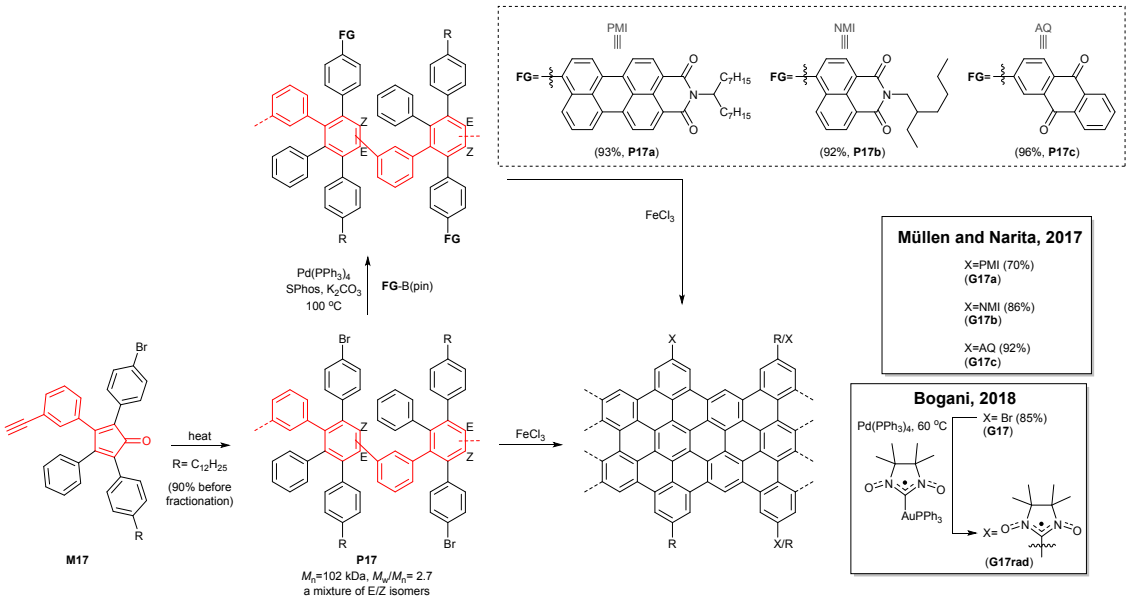

Fig. 16 Edge functionalisation of cove-type GNRs.

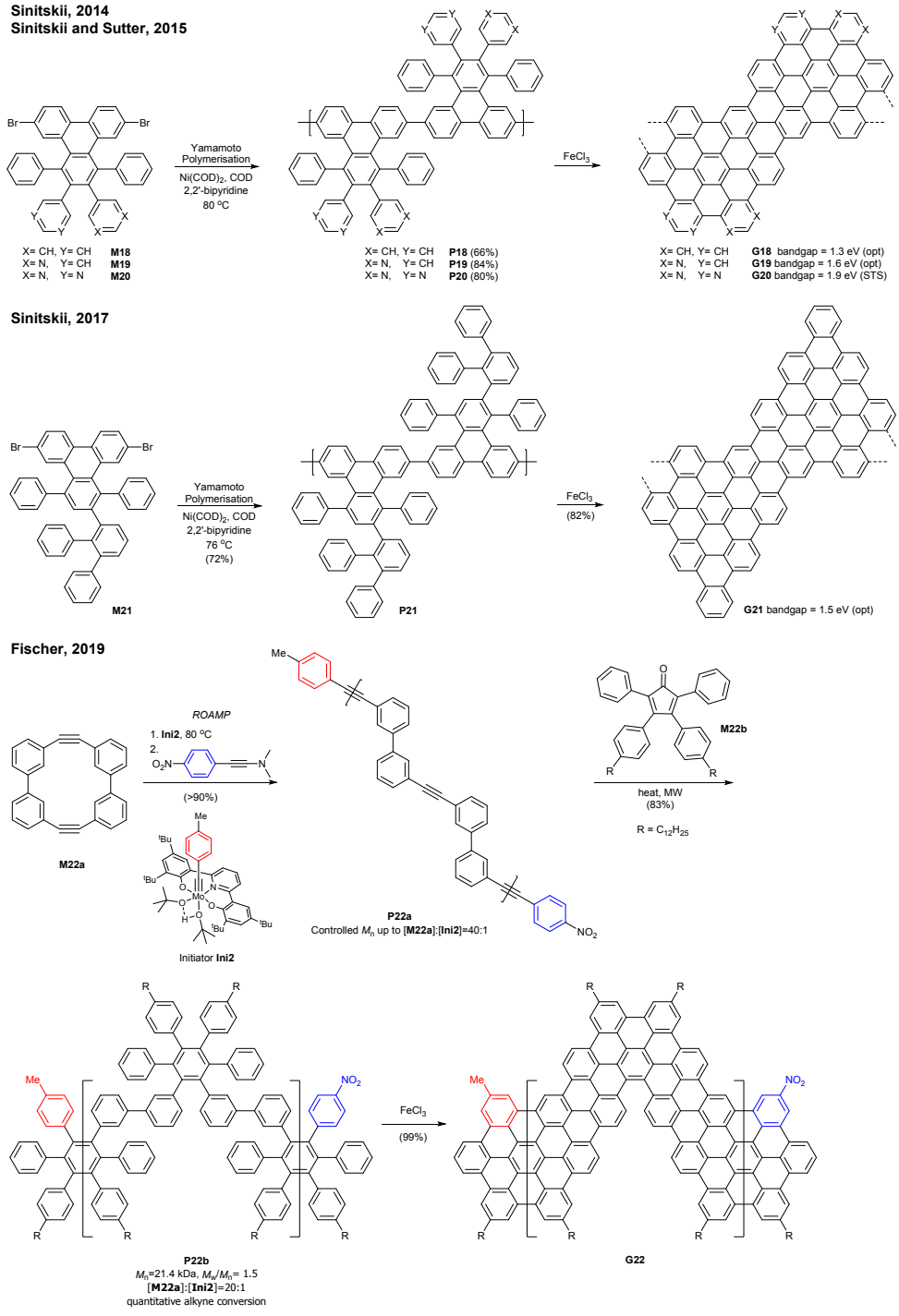

Fig. 17 Synthesis of chevron-type GNRs.

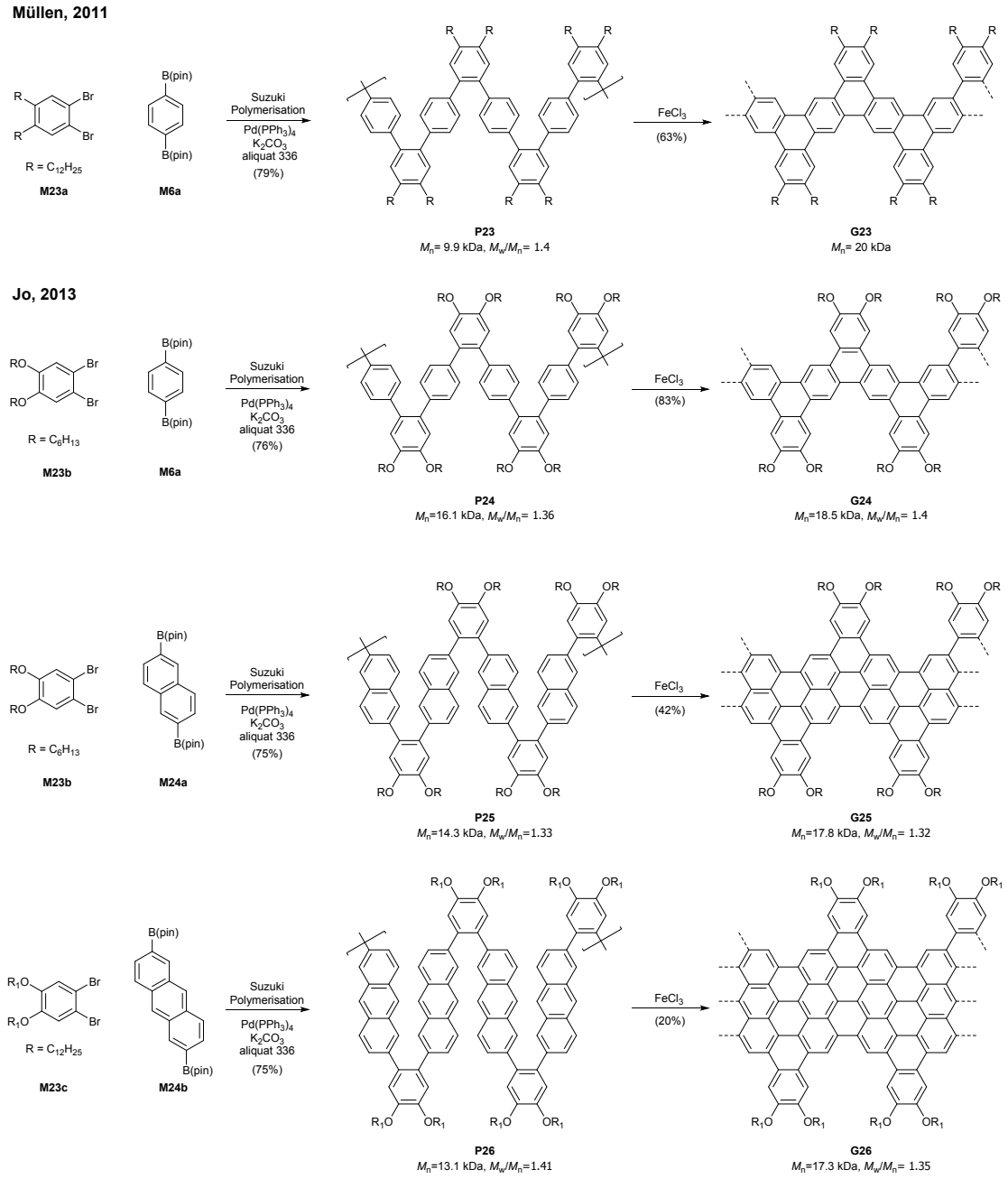

Fig. 18 Synthesis of soluble “kinked” GNRs.

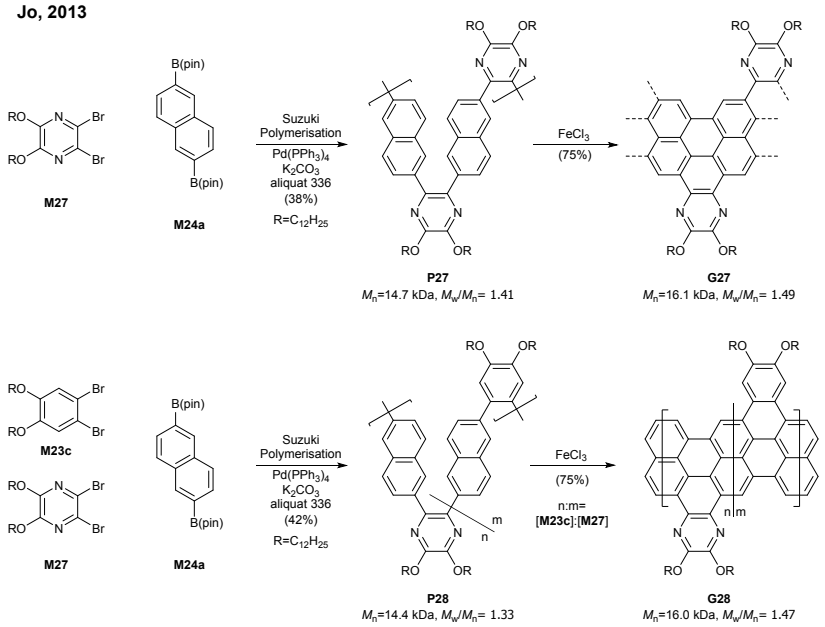

Fig. 19 Synthesis of nitrogen-doped "kinked" GNRs.

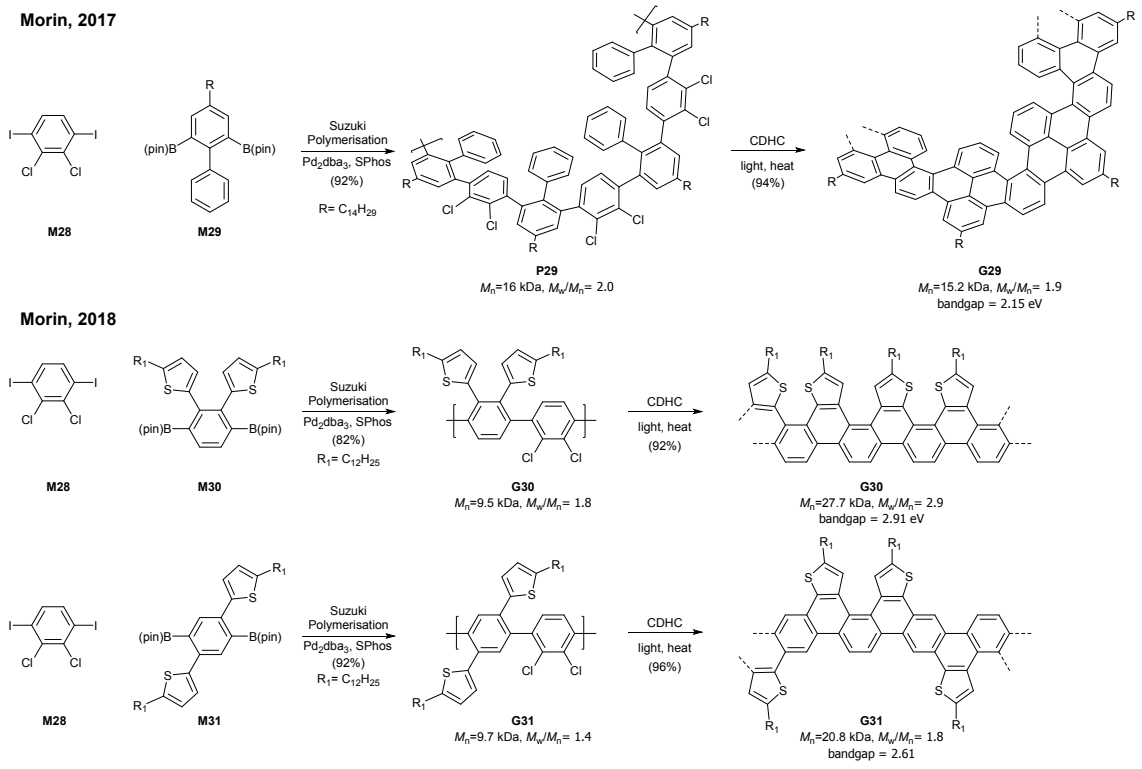

Fig. 20 Synthesis of fjord-type GNRs.

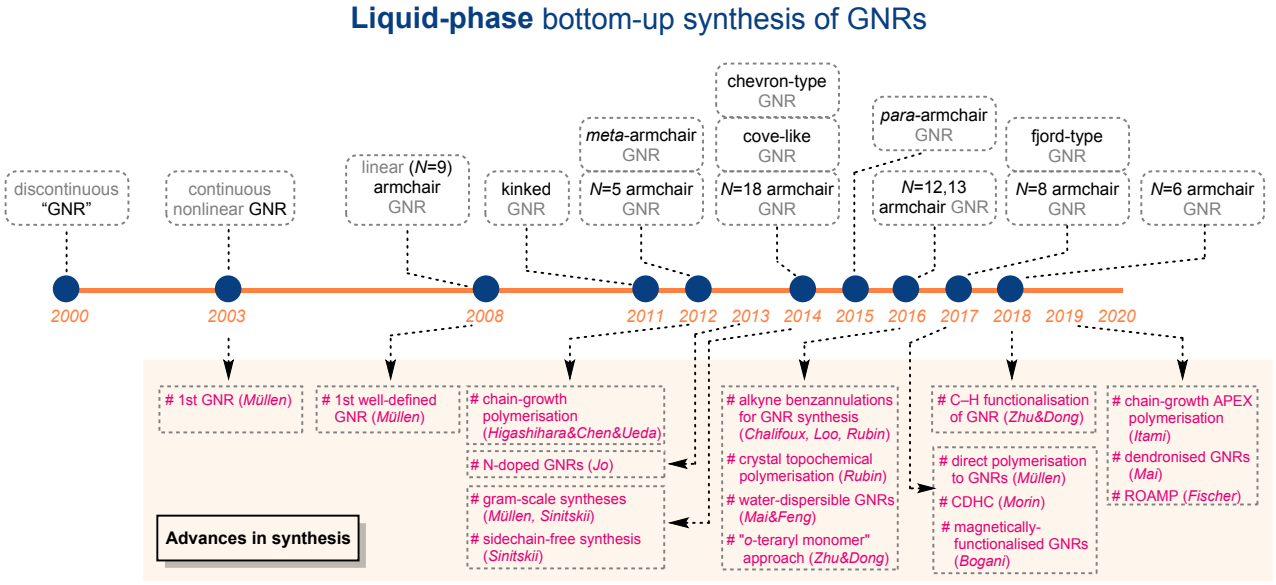

Fig. 21. A timeline of liquid-phase bottom-up synthesis of GNRs.

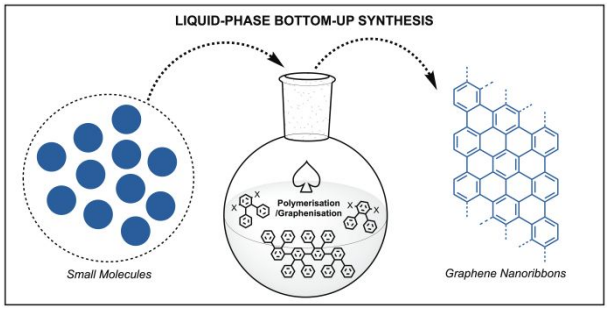

This review summarises the development of bottom-up synthesis of graphene nanoribbons in liquid phase and provides views on challenges in the field and the future outlook.